Studies of $\sigma(e^+e^- \to \text{hadrons})$ at BABAR using Initial State Radiation (ISR)

W. F. Wang[a]

[a]Representing the *BABAR* Collaboration
Laboratoire de l'Accelerateur Lineaire,Orsay,France
E-mail: wangwf@lal.in2p3.fr

We present a review of BaBar results on $e^+e^- \to$ hadrons using the initial state radiation technique. Cross sections over the $\sqrt{s}$ range from threshold to $4-5$ GeV, with very small point-to-point systematic errors, are presented for the $\pi^+\pi^-\pi^0$, $2(\pi^+\pi^-)$, $2(K^+K^-)$, $3(\pi^+\pi^-)$, $2(\pi^+\pi^-)2\pi^0$, $2(\pi^+\pi^-)K^+K^-$, and $p\overline{p}$ final states . The preliminary results of $e^+e^- \to K^+K^-\pi^+\pi^-$ and $e^+e^- \to K^+K^-\pi^0\pi^0$ cross sections are also presented.

1. Introduction

The precise measurements of $R = \frac{\sigma(e^+e^- \to \text{hadrons})}{\sigma(e^+e^- \to \mu^+\mu^-)}$ are crucial input for calculating the hadronic contribution to 1) the muon anomalous magnetic moment [1] and 2) the running of the electromagnetic coupling α_{QED} [2]. The interest in this kind of study has been increasing because of discrepancy between the measured muon $g-2$ value [3] and the one predicted by the Standard Model (see presentation by M. Davier), where the hadronic contribution to the prediction is taken from e^+e^- experiments at low energies or the spectra function of τ decays. The *BABAR* [4] collaboration has an intensive program for a study of the low energy cross sections and hadron spectroscopy via ISR, and several multi-hadron cross sections have been measured[5–7], benefiting from the good BABAR detector performance and particle identification capabilities.

The BABAR detector is described elsewhere [4]. Charged-particle tracking is provided by a five-layer silicon vertex tracker (SVT) and a 40-layer drift chamber (DCH), operating in a 1.5-T axial magnetic field. The transverse momentum resolution is 0.47% at 1 GeVc. Energies of photons are electrons are measured with a CsI(T1) electromagnetic calorimeter (EMC) with a resolution of 3% at 1 GeV. Charged particle identification is provided by ionization measurements in the SVT and DCH, and by an internally reflecting ring-imaging Cherenkow detector (DIRC). Muons are identified in the solenoid's instrumented flux return, which consisits of iron plates interleaved with resistive plate chambers.

2. The ISR method

The ISR cross section for a particular final state f depends on e^+e^- cross section $\sigma_f(s)$ and is obtained from:

$$\frac{d\sigma(s,x)}{dx} = W(s,x) \cdot \sigma_f(s(1-x)), \qquad (1)$$

where $x = \frac{2E_\gamma}{\sqrt{s}}$; E_γ is the energy of the ISR photon in the c.m. frame, and $\sqrt{s}$ is the nominal c.m. energy. The function $W(s,x)$ describes the energy spectrum of the virtual photons and can be calculated with better than 1% accuracy[9–11]. ISR photons are produced at all angles relative to the collision axis. The *BABAR* acceptance for such photons is around 10 %. An advantage deriving from the use of ISR is that the entire range of effective collision energy is scanned in one experiment. This avoids the relative normalization uncertainties which can arise when data from different experiments are combined. A disadvantage is that the invariant mass resolution of about 8 MeV limits the width of the narrowest structure

which can be measured via ISR production. Nevertheless it's sufficient to observe the J/ψ production and measure the product $\Gamma \cdot B_{ee} \cdot B_f$ where Γ and B_{ee}, B_f are the total width, branching fractions of J/ψ to e^+e^- and final state f.

3. $e^+e^- \rightarrow \pi^+\pi^-\pi^0$, $\pi^+\pi^-\pi^+\pi^-$ and $K^+K^-\pi^+\pi^-$

The $\pi^+\pi^-\pi^0$, $2(\pi^+\pi^-)$ and $K^+K^-\pi^+\pi^-$ final states have been studied using 89 fb^{-1} of *BABAR* luminosity and published in details in Ref. [5,6].
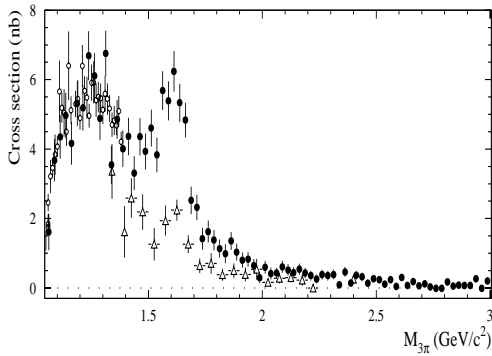

Figure 1. The $e^+e^- \rightarrow \pi^+\pi^-\pi^0$ cross section measured by *BABAR* (filled circles), by SND (open circles), and DM2 (open triangles).

The $e^+e^- \rightarrow \pi^+\pi^-\pi^0$ cross section in the 1.05-3.0 GeV/c^2 region is presented in Fig. 1. It is in agreement with the SND data, but in contradiction with the DM2 measurements. The systematic errors are around 5%. Only statical errors are shown here, which is same for all cross section plots. The structures at 1.25 GeV and 1.65 GeV are well fitted to ω' and ω'' resonances.

Fig. 2 presents the $e^+e^- \rightarrow \pi^+\pi^-\pi^+\pi^-$ cross section [6] obtained by *BABAR* in comparison with all existing e^+e^- data. It is consistent with previous results, and BABAR has the best measurement for > 1.4 GeV. The systematic errors are around 5%. The oberved cross section prefer quasi-two-body production of $a_1(1260)\pi$. The
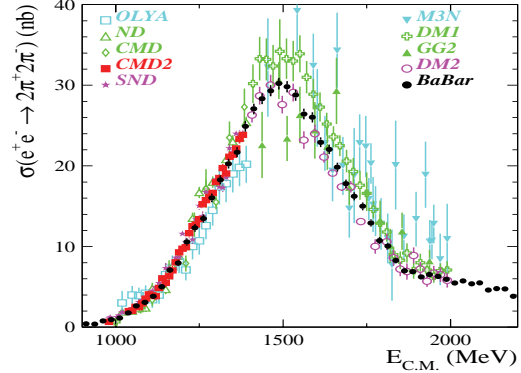

Figure 2. The $e^+e^- \rightarrow \pi^+\pi^-\pi^+\pi^-$ cross section obtained from ISR at *BABAR* in comparison with all e^+e^- data.

substructure study also shows an indication of $f_0(1370)\rho(770)$ contribution to the final state.

4. $e^+e^- \rightarrow 3(\pi^+\pi^-)$, $2(\pi^+\pi^-)\pi^0\pi^0$ and $K^+K^-2(\pi^+\pi^-)$

Also published are the cross sections for the $e^+e^- \rightarrow 3(\pi^+\pi^-)$ and $e^+e^- \rightarrow 2(\pi^+\pi^-)\pi^0\pi^0$ final states obtained from 232 fb^{-1} of *BABAR* data [7] and shown in Fig. 3. Their systematic errors are about 6% and 10% respectively. Compared with previous measurements, their accuracies are largely improved and cover a larger energy range. A dip at ~ 1.9 GeV is seen in both channels, as already observed by DM2[12] and FOCUS [15]. The $\pi^+\pi^-$ decay of the ρ dominates the substructure observed in the $3(\pi^+\pi^-)$ final state, with little evidence for any other structures. However, $\rho 4\pi$, $\omega\pi^+\pi^-\pi^0$ and $\omega\eta$ all have contributions to the $2(\pi^+\pi^-)\pi^0\pi^0$ final state.

The cross section of hadronic final state $K^+K^-2(\pi^+\pi^-)$ is also presented for the first time.

5. Preliminary results of $e^+e^- \rightarrow K^+K^-\pi^+\pi^-$ and $e^+e^- \rightarrow K^+K^-\pi^0\pi^0$ final states

Here we present an update of our previous analysis [6] of $e^+e^- \rightarrow K^+K^-\pi^+\pi^-$ and the
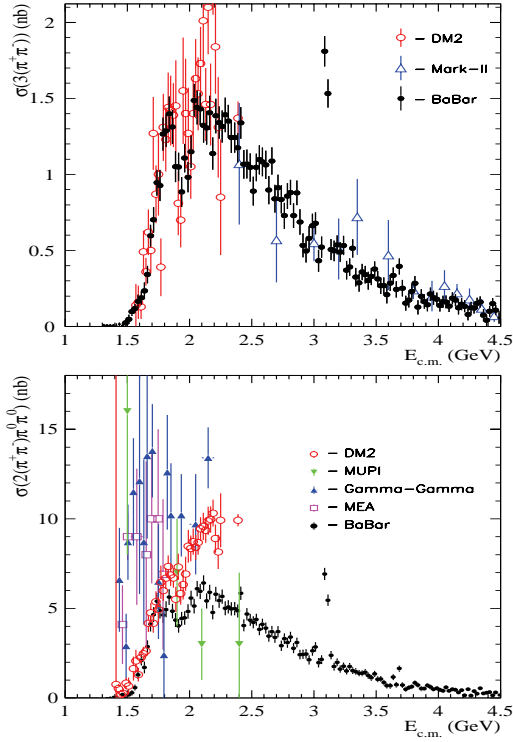
Figure 3. The (top) $e^+e^- \to 3(\pi^+\pi^-)$ and (bottom) $e^+e^- \to 2(\pi^+\pi^-)\pi^0\pi^0$ cross sections in comparison with direct e^+e^- measurements.

Figure 4. The (a) $e^+e^- \to K^+K^-\pi^+\pi^-$ and (b) $e^+e^- \to K^+K^-\pi^0\pi^0$ cross sections as a function of e^+e^- C.M. energy in comparison with previous DM1 experiment (open circles).

first measurement of $e^+e^- \to K^+K^-\pi^0\pi^0$. Due to more statics and the optimization of the criteria, the number of selected $K^+K^-\pi^+\pi^-$ events is increased by a factor of 5. In Fig. 4 we show the cross sections for the $e^+e^- \to K^+K^-\pi^+\pi^-$ and $e^+e^- \to K^+K^-\pi^0\pi^0$ processes vs. $E_{C.M.}$. The total systematic uncertainty in the $K^+K^-\pi^+\pi^-(\pi^0\pi^0)$ cross section ranges from 7% (10%) at threshold to 9% (15%) at high $E_{C.M.}$. These processes are dominated by the intermediated states with $K^*(892)$ [6] with a small fraction associated with the $\phi(1020)$ production.

Selecting ϕ events (see Figs. 5(a,c)) and subtracting side-band and MC simulated backgrounds, we obtain the ϕ-associated $m(\pi\pi)$ distributions shown in Figs. 5(b,d). Clear $f_0(980)$ signals are visible in both cases. We obtain two
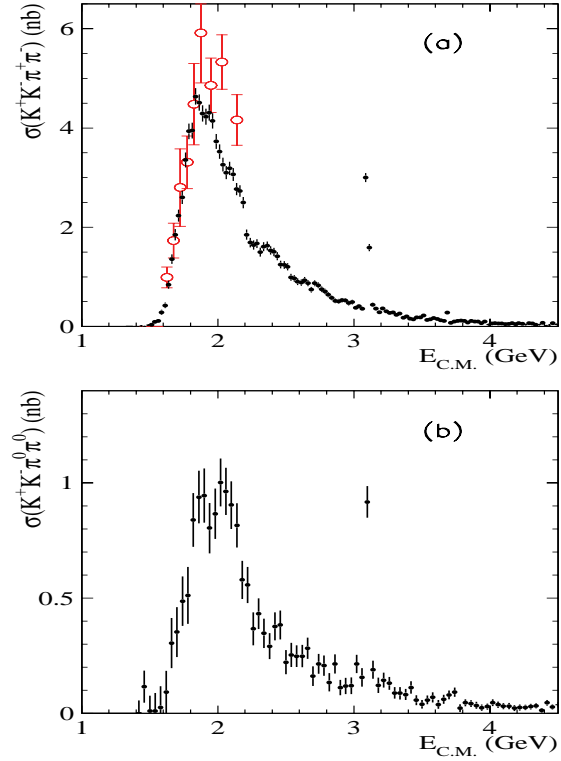
consistent measurements of the $e^+e^- \to \phi f_0$ cross section shown in Fig. 6. The structure at 2.1 GeV is fitted by assuming a resonance over continuum production. The fitted resonance parameters are $m_x = 2.175 \pm 0.010 \pm 0.015 \, \text{GeV}/c^2$, $\Gamma_x = 0.058 \pm 0.016 \pm 0.020 \, \text{GeV}/c^2$.

6. $e^+e^- \to p\overline{p}$

The cross section for $e^+e^- \to p\overline{p}$ depends on two form factors: electric (G_E) and magnetic (G_M). The ratio of the form factors can be extracted from the analysis of the decay angle distribution in the $p\overline{p}$ rest frame. The G_E distribution is close to $\sin^2\theta$, the G_M distribution to $1+\cos^2\theta$. The obtained mass dependence of $|G_E/G_M|$ is
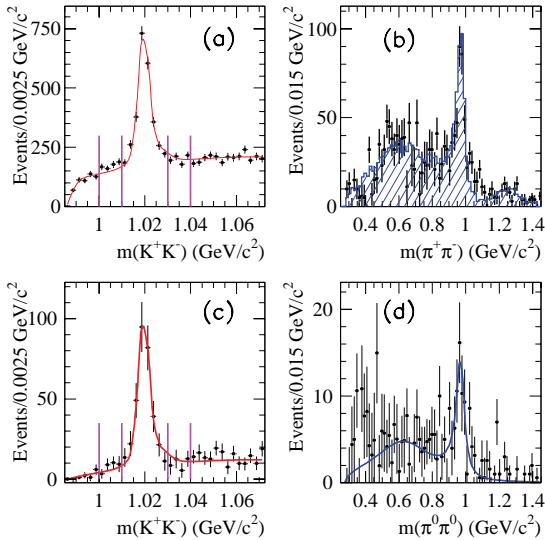
Figure 5. The $m(K^+K^-)$ projections for the (a) $K^+K^-\pi^+\pi^-$ and (c) $K^+K^-\pi^0\pi^0$ candidates in the data. The vertical lines delimit ϕ signal and sideband regions. (b,d) $m(\pi\pi)$ distribution for events in the ϕ signal region of (a,c) minus that for events in the sidebands. The curves (histogram) represent the results of the fits (simulation) described in the text.
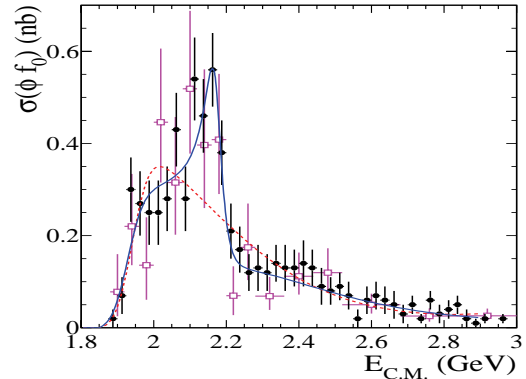

Figure 6. The $e^+e^- \to \phi(1020)f_0(980)$ cross section obtained via ISR in the $K^+K^-\pi^+\pi^-$ (circles) and $K^+K^-\pi^0\pi^0$ (squares) final states.
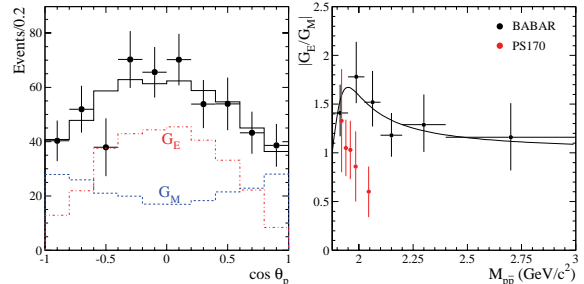

Figure 7. The $cos\theta$ distribution (left), and mass dependence of the ratio $|G\_E/G\_M|$ (right).

shown in Fig. 7. Our result disagrees significantly with the previous measurement from LEAR[14].

From measuring the total cross section, we can extract a combination of form factor. We define the effective form factors as $F(m) = \sqrt{(|G_M(m)|^2) + \frac{2m_p^2}{m^2}|G_E(m)|^2)/(1 + \frac{2m_p^2}{m^2})}$. Such a definition allows to compare our form factor results with the data from previous e^+e^- and $p\overline{p}$ experiments which use the assumption that $|G_E| = |G_M|$. The near-threshold enhancement of form factor is confirmed, two sharp drops of the form factor(at ~ 2.25 GeV and ~ 3 GeV) show some structures. The higher mass region is in agreement with pQCD prediction.

7. J/ψ and $\psi(2S)$ production

The J/ψ decay rates have been measured for all above final states, their branching fractions are calculated as the following:

$$B_f(J/\psi \to f) \cdot \Gamma_{ee}^{J/\psi} = \frac{N(J/\psi \to f) \cdot m_{J/\psi}^2}{6\pi^2 \cdot d\mathcal{L}/dm \cdot \epsilon_{MC} \cdot C} \quad (2)$$

$N(J/\psi \to f)$ is the observed number of events for the process of $e^+e^- \to f$; $\Gamma_{ee}^{J/\psi}$ is the electronic width of J/ψ taken from PDG 2004; $d\mathcal{L}/dm$ is the ISR luminosity at the J/ψ mass; ϵ_{MC} is the detection efficiency; and $C = 3.894 \times 10^{11}$nbMeV^2 is a conversion constant.

Table 1
The summary of $B_f(J/\psi \rightarrow f)$

f	BABAR (%)	PDG-2004 (%)	BESII (%)
$\pi^+\pi^-\pi^0$	2.18 ± 0.19	1.50 ± 0.20	2.09 ± 0.12
$\pi^+\pi^-\pi^+\pi^-$	0.361 ± 0.037	0.40 ± 0.10	0.353 ± 0.031
$K^+K^-\pi^+\pi^-$	0.609 ± 0.073	0.720 ± 0.230	
$\phi\pi^+\pi^-$	0.098 ± 0.013	0.080 ± 0.012	0.109 ± 0.013
$\phi\pi^0\pi^0$	0.585 ± 0.162	-	
$3(\pi^+\pi^-)$	0.440 ± 0.041	0.40 ± 0.20	-
$2(\pi^+\pi^-\pi^0)$	1.65 ± 0.21	-	
$\omega\eta$	0.147 ± 0.044	0.158 ± 0.016	
$K^+K^-K^+K^-$	0.67 ± 0.14	-	
$K^+K^-2(\pi^+\pi^-)$	0.509 ± 0.055	0.31 ± 0.13	
$\phi 2(\pi^+\pi^-)$	0.177 ± 0.037	0.162 ± 0.032	
$p\overline{p}$	2.22 ± 0.16	2.17 ± 0.08	

Table 2
The summary of $B_f(\psi(2S) \rightarrow f)$

f	BABAR BF($\times 10^{-3}$)	PDG 2004($\times 10^{-3}$)
$2(\pi^+\pi^-\pi^0)$	5.3 ± 0.17	-
$K^+K^-2(\pi^+\pi^-)$	2.1 ± 1.0	-
$p\overline{p}$	0.33 ± 0.09	0.236 ± 0.024

Table 1 and table 2 show BABAR has competitive results for most of channels. BABAR result on $J/\psi \rightarrow \pi^+\pi^-\pi^0$ is in disagreement with the values in PDG 2004, but good agree with the new values of BESII.

8. Conclusion

A number of ISR processes have been studied with a 232 fb^{-1} (or 89 fb^{-1}) data sample in the *BABAR* detector, their cross sections are presented. The cross sections of $e^+e^- \rightarrow 2(K^+K^-)$, $K^+K^-\pi^0\pi^0$, ϕf^0 and $2(\pi^+\pi^-)K^+K^-$ are the first measurements. The results of $2(\pi^+\pi^-)$, $3(\pi^+\pi^-)$, $p\overline{p}$ and $K^+K^-\pi^+\pi^-$ are consistent with previous results, but cover a larger energy range. The values of $e^+e^- \rightarrow \pi^+\pi^-\pi^0$ are agree with SND for lower mass region, disagree with DM2 for higher mass region. For $e^+e^- \rightarrow 2(\pi^+\pi^-)2\pi^0$, BABAR and DM2 only agree for mass less 1.8 GeV. Radiative return to the J/ψ resonance allows the measurements of a number of relative branching fractions more precisely than earlier measurements.

The BABAR collaboration provide high statistics measurements of exclusive hadronic cross sections with $(5-10)\%$ systematic uncertainties. It largely improve the precision of R over the existing data in the range larger than 1.4 GeV [1].

REFERENCES

1. M. Davier *et al.*, *Eur. Phys. J.*, **C27**,497 (2003).
2. H. Burkhardt and B. Pietrzyk, *Phys. Lett.* **B513** 46(2001).
3. G. W. Bennett *et al.*, *Phys. Rev.* **D73** 072003(2006).
4. *BABAR* Collaboration, B. Aubert *et al.*, *Nucl. Instr. and Meth.* **A479**, 1 (2002).
5. *BABAR* Collaboration, B. Aubert *et al.*, *Phys. Rev.* **D70**, 072004 (2004).
6. *BABAR* Collaboration, B. Aubert *et al.*, *Phys. Rev.* **D71**, 052001 (2005).
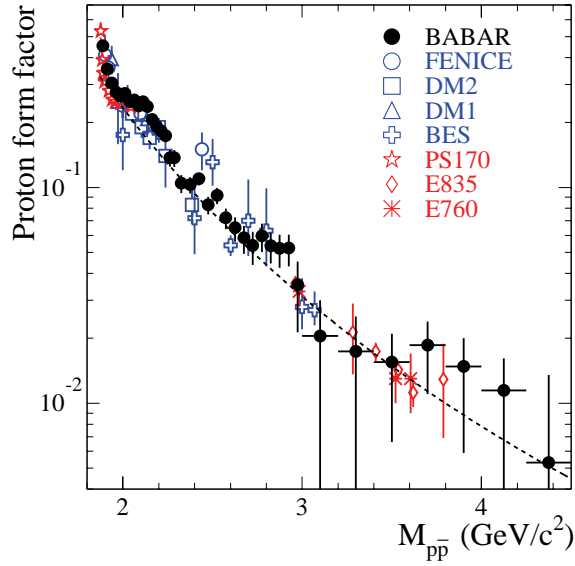7. *BABAR* Collaboration, B. Aubert *et al.*, *Phys. Rev.* **D73**, 052003 (2006).

Figure 8. The effective proton form factor as a function of e^+e^- C.M. energy. The curve is the pQCD prediction.

8. *BABAR* Collaboration, B. Aubert *et al.*, *Phys. Rev.* **D73**, 012005 (2006).

9. A.B. Arbuzov *et al.*, *JHEP* **9812**, 009 (1998).

10. S. Binner, J.H. Kuehn and K. Melnikov, *Phys. Lett.* **B459** 279 (1999).

11. M. Benayoun *et al.*, *Mod. Phys. Lett.* **A14**, 2605 (1999).

12. A. Antonelli *et al.*,*Z. Phys.* **C56**, 15 (1992)

13. Review of Particle Physics, W.-M. Yao *et al.*, *Journal of Physics G.* **33**, 1 (2006).

14. G. Bardin *et al.*, *Nucl. Phys.* B 411, 3 (1994).

15. P. L. Frabetti *et al.*, *Phys. Lett.* **B514**, 240 (2001).